J Geod (2005) 79: 135–145
DOI 10.1007/s00190-005-0452-3

ORIGINAL ARTICLE

J. Huang · M. Véronneau

Applications of downward-continuation in gravimetric geoid modeling: case studies in Western Canada

Received: 20 April 2004 / Accepted: 6 October 2004 / Published online: 19 May 2005

Abstract The objective of this study is to evaluate two approaches, which use different representations of the Earth's gravity field for downward continuation (DC), for determining Helmert gravity anomalies on the geoid. The accuracy of these anomalies is validated by 1) analyzing conformity of the two approaches; and 2) converting them to geoid heights and comparing the resulting values to GPS-leveling data. The first approach (A) consists of evaluating Helmert anomalies at the topography and downward-continuing them to the geoid. The second approach (B) downward-continues refined Bouguer anomalies to the geoid and transforms them to Helmert anomalies by adding the condensed topographical effect. Approach A is sensitive to the DC because of the roughness of the Helmert gravity field. The DC effect on the geoid can reach up to 2 m in Western Canada when the Stokes kernel is used to convert gravity anomalies to geoid heights. Furthermore, Poisson's equation for DC provides better numerical results than Moritz's equation when the resulting geoid models are validated against the GPS-leveling. On the contrary, approach B is significantly less sensitive to the DC because of the smoothness of the refined Bouguer gravity field. In this case, the DC (Poisson's and Moritz's) contributes only at the decimeter level to the geoid model in Western Canada. The maximum difference between the geoid models from approaches A and B is about 5 cm in the region of interest. The differences may result from errors in the DC such as numerical instability. The standard deviations of the $h - H - N$ for both approaches are about 8 cm at the 664 GPS-leveling validation stations in Western Canada.

J. Huang (✉) · M. Véronneau
Geodetic Survey Division, CCRS,
Natural Resources Canada
615 Booth Street, Ottawa,
ON, Canada, K1A 0E9
Tel.: +1-613-947-1043 (JH), +1-613-992-1988 (MV)
Fax: +1-613-992-6628
E-mail: jianhuan@nrcan.gc.ca, marcv@nrcan.gc.ca

Keywords Downward continuation (DC) · Geoid · Condensed topographical effect (CTE) · Primary indirect topographical effect (PITE)

1 Introduction

For decades, studies of the downward continuation (DC) of potential and gravity fields have continuously attracted geodesists' attention because of its essential role in physical geodesy and mathematical difficulty (e.g., Heiskanen and Moritz 1967; Schwarz 1978; Moritz's 1980; Jekeli 1981; Bjerhammar 1987; Sideris 1987; Wang 1988; Engels et al. 1993; Sjöberg 1996; Vaníček et al. 1996; Martinec 1996; Sun and Vaníček 1998; Sjöberg 1998; Milbert 1999; Nahavandchi 2000; Wong 2001; Novák and Heck 2001; Ilk et al. 2002; Sjöberg 2003; Jekeli and Serpas 2003; Huang et al. 2003a). Downward continuation constitutes a basic reduction step in solving the geodetic boundary-value problem (GBVP), i.e., gravity values measured on or above the Earth's surface must be continued downward to the boundary (geoid). However, the fact that DC is classified as an ill-posed problem in mathematics has limited its practical applications (e.g., Schwarz 1978; Rummel et al. 1979; Engels et al. 1993; Martinec 1996; Ilk et al. 2002).

Instead, DC was either approximated or simply neglected in gravity reduction, despite a great amount of literature on the topic (e.g., Moritz's 1980; Wang 1988; Véronneau 1997; Omang and Forsberg 2000). Over the last ten years, important progress has been made in the development of numerical methods for DC. Its instability has been numerically analyzed and characterized to support geoid determination at the centimeter level. In addition, numerical techniques and algorithms have been developed to accurately and efficiently evaluate the contribution of the DC (Vaníček et al. 1996; Martinec 1996; Sun and Vaníček 1998; Wong 2001; Novák and Heck 2001; Huang 2002).

In the last decade, Stokes's method for gravimetric geoid modeling based on Helmert's second method of condensation (Heiskanen and Moritz 1967; Martinec et al.

1993; Heck 2003) has become accepted as one of the mainstream methods for regional geoid modeling (e.g., Vaníček and Martinec 1994; Sideris 1994; Véronneau 1997; Smith and Milbert 1999; Featherstone et al. 2001). This method requires Helmert gravity anomalies on its co-geoid as boundary values (Vaníček et al. 1999). There are basically two procedures to follow in evaluating the Helmert gravity anomalies on the co-geoid:

(A) the Helmert gravity anomalies are evaluated on or above the irregular Earth's surface, then are continued downward to the geoid, i.e., the masses above the geoid are removed and condensed as a mass layer on the geoid prior to the DC (Heiskanen and Moritz 1967; Vaníček et al. 1996; Martinec 1996; Nahavandchi 2000);

(B) the refined (or complete) Bouguer anomalies on or above the surface of the Earth are downward continued to the geoid, then the Helmert gravity anomalies are evaluated on the geoid, i.e., the mass condensation is carried out as a post-DC step (Moritz 1968; Sideris 1994; Véronneau 2002).

Strictly speaking, the Helmert anomalies must then be continued to the co-geoid from the geoid for both approaches. However, this reduction is usually negligible (Vaníček et al. 1999). Until recently, the DC was considered negligible in most applications when following approach B in terms of either its small magnitude or tests against GPS-leveling data (see, e.g., Sideris 1994; Véronneau 1997; Omang and Forsberg 2000).

The two approaches (A and B) are equivalent in theory, but in practice they have their advantages and disadvantages. Approach A is physically straightforward and the far-zone contribution of the DC is negligible (Huang 2002), but it demands a fair amount of effort to evaluate the condensed topographical effect (CTE) on or above the Earth's surface. In addition, the DC may be unstable because of the roughness of the Helmert gravity field and data errors (Martinec 1996). On the other hand, approach B is efficient in regard to the evaluation of the CTE and the stability of the DC. Its contribution is relatively small in magnitude. However, the DC of the refined Bouguer anomalies requires a global integration because the far-zone still contributes significantly.

Jekeli and Serpas (2003) numerically compare the same two approaches in three regions with different topographies. In the two regions with relatively smooth topography, both approaches gave similar geoid solutions because the DC is small. In the rugged region, the two approaches gave significantly different geoid solutions. The difference gave rise to uncertainty about the stability of the DC in mountainous regions.

There are two well-known harmonic methods for evaluating the DC: Poisson's (Heiskanen and Moritz 1967) and Moritz's (1980). The former is based on Poisson's integral, while the latter is formulated as a Taylor-series-like expression. Huang et al. (2003a) numerically compare the two methods in the Canadian Rocky Mountains. They show that Moritz's method yields approximation errors that account for about 10% of the DC, which is equivalent to a geoid effect of 20 cm for approach A in the Canadian Rocky Mountains.

In this paper, the two procedures described above are used for determining Helmert gravity anomalies on the geoid in Western Canada, where the magnitude of the DC is the largest in Canada. The DC is evaluated using Poisson's and Moritz's methods. The geoid models resulting from each combination of the two approaches (A and B) and the two DC methods (Poisson and Moritz) are compared to GPS-leveling data in Western Canada.

2 Two approaches for the determination of boundary values in the Stokes-Helmert scheme

There are three options to determine Helmert gravity anomalies on the geoid. The first procedure consists of removing the topography and restoring it as a condensed mass layer below the geoid prior to downward-continuing the anomaly to the geoid (e.g. Vaníček et al. 1999). The second procedure consists of removing the topography, downward-continuing the anomaly to the geoid and restoring the condensed mass below the geoid (e.g. Sideris 1994). Finally, the third option may consist of downward-continuing the anomaly through the topography to the geoid, removing the topography and restoring it as a condensed mass layer below the geoid. However, the third option is more complex because it does not derive a harmonic field for the downward continuation. Consequently, we will only consider the first two options.

2.1 Approach A

The anomalous potential T is defined as (Heiskanen and Moritz 1967):

$$T(r, \Omega) = W(r, \Omega) - U(r, \Omega) \tag{1}$$

where r is the geocentric radius; Ω is the geocentric angle denoting the pair (θ, λ), the spherical co-latitude and longitude; W and U represent the earth's gravity potential and the normal gravity potential of the reference ellipsoid, respectively.

According to Helmert's second condensation, the anomalous potential T_{H} is defined as

$$T_{\mathrm{H}}(r, \Omega) = T(r, \Omega) - \delta V_{\mathrm{t}}(r, \Omega) \tag{2}$$

The residual topographical potential δV_{t} is defined as

$$\delta V_{\mathrm{t}}(r, \Omega) = V_{\mathrm{t}}(r, \Omega) - V_{\mathrm{ct}}(r, \Omega) \tag{3}$$

where V_{t} represents the topographical potential, and V_{ct} represents the condensed topographical potential.

The Helmert gravity anomaly Δg_{H} for centimeter geoid determination on and above the earth's surface is given by (Vaníček et al. 1999):

$$\Delta g_{\mathrm{H}}(r, \Omega) = \Delta g(\Omega) + \frac{2}{R} H(\Omega) \Delta g_{\mathrm{B}}(\Omega) + \frac{\partial V_{\mathrm{t}}(r, \Omega)}{\partial h} - \frac{\partial V_{\mathrm{ct}}(r, \Omega)}{\partial h} + \delta\gamma + \delta A^{\mathrm{a}} \tag{4}$$

where Δg is the free-air gravity anomaly; the second term is a correction for the separation between the quasigeoid and the geoid; the third term contains the Bouguer shell and spherical terrain corrections; the fourth term contains the condensed Bouguer shell and spherical terrain corrections; $\delta\gamma$ is the secondary indirect topographical effect (SITE); δA^{a} is the direct atmospheric effect; H is the orthometric height of the topography; and Δg_{B} is the simple planar Bouguer gravity anomaly.

As for the actual Earth, the fundamental equation of physical geodesy can also be expressed for Helmert's disturbing potential T_{H} on and above the Earth's surface (Heiskanen and Moritz 1967; Vaníček et al. 1999):

$$\left(-\frac{\partial T_{\mathrm{H}}(r,\Omega)}{\partial h}+\frac{T_{\mathrm{H}}(r,\Omega)}{\gamma(r,\Omega)}\frac{\partial\gamma(r,\Omega)}{\partial h}\right)=\Delta g_{\mathrm{H}}(r,\Omega)+\epsilon, \tag{5}$$

where ϵ stands for the correction for deflection of the vertical, and γ stands for the normal gravity. Because the boundary values are required on the geoid, the Helmert gravity anomalies evaluated from the data must be reduced to the geoid. The most common reduction technique is the spherical harmonic DC for which Eq. (5) must be written in its spherical approximation as follows:

$$\left(-\frac{\partial T_{\mathrm{H}}(r,\Omega)}{\partial r}-\frac{2}{r}T_{\mathrm{H}}(r,\Omega)\right)\doteq\Delta g_{\mathrm{H}}(r,\Omega)\,. \tag{6}$$

Equation (6) allows us to use the harmonic DC technique to reduce the Helmert gravity anomalies to the geoid because $r\Delta g_{\mathrm{H}}$ becomes harmonic. Therefore, we have

$$\Delta g_{\mathrm{H}}(r_{\mathrm{g}},\Omega)\doteq\Delta g_{\mathrm{H}}(r,\Omega)+f_{\mathrm{DC}}(\Delta g_{\mathrm{H}}(r,\Omega))\,, \tag{7}$$

where r_{g} stands for the geocentric radius of a point on the geoid; f_{DC} corresponds to the DC operator. Numerical experiments show that the DC effect of the Helmert gravity anomalies on the geoid does not exceed 3 m in the region of interest. It is therefore predictable that the error from the spherical harmonic DC is less than 1 cm.

2.2 Approach B

Equation (5) can be re-written into a form to satisfy a modeled Earth where all the topography is removed, i.e., a spherical refined Bouguer (SRB) gravity field

$$\left(-\frac{\partial T_{\mathrm{SRB}}(r,\Omega)}{\partial h}+\frac{T_{\mathrm{H}}(r,\Omega)}{\gamma(r,\Omega)}\frac{\partial\gamma(r,\Omega)}{\partial h}\right)=\Delta g_{\mathrm{SRB}}(r,\Omega)+\epsilon\,, \tag{8}$$

where

$$T_{\mathrm{SRB}}(r,\Omega)=T_{\mathrm{H}}(r,\Omega)-V_{\mathrm{ct}}(r,\Omega) \tag{9}$$

and

$$\Delta g_{\mathrm{SRB}}(r,\Omega)=\Delta g(\Omega)+\frac{2}{R}H(\Omega)\Delta g_{\mathrm{B}}(\Omega)+\frac{\partial V_{\mathrm{t}}(r,\Omega)}{\partial h}+\delta\gamma+\delta A^{\mathrm{a}}\,. \tag{10}$$

The SRB gravity anomaly defined in Eq. (10) differs from the Helmert gravity anomaly in Eq. (4) by only the condensed topographical effect (CTE). The CTE is defined in Appendix A. Equation (8) can be written in the following form by spherical approximation

$$\left(-\frac{\partial T_{\mathrm{SRB}}(r,\Omega)}{\partial r}-\frac{2}{r}T_{\mathrm{H}}(r,\Omega)\right)\doteq\Delta g_{\mathrm{SRB}}(r,\Omega)\,. \tag{11}$$

Equation (11) makes the spherical harmonic DC possible because $r\Delta g_{\mathrm{SRB}}$ becomes harmonic. Thus, we have

$$\Delta g_{\mathrm{SRB}}(r_{\mathrm{g}},\Omega)\doteq\Delta g_{\mathrm{SRB}}(r,\Omega)+f_{\mathrm{DC}}(\Delta g_{\mathrm{SRB}}(r,\Omega))\,, \tag{12}$$

and

$$\Delta g_{\mathrm{H}}(r_{\mathrm{g}},\Omega)\doteq\Delta g_{\mathrm{SRB}}(r,\Omega)+f_{\mathrm{DC}}(\Delta g_{\mathrm{SRB}}(r,\Omega))-\left.\frac{\partial V_{\mathrm{ct}}(r,\Omega)}{\partial h}\right|_{r=r_{\mathrm{g}}}. \tag{13}$$

Numerical experiments show that the DC of the refined Bouguer gravity anomalies on the geoid does not exceed 0.5 m in the region of interest. Thus, the error from the spherical harmonic DC is at the sub-centimeter level. Different authors have described this approach with different approximations (Moritz 1968; Sideris 1994; Véronneau 2002).

From Eqs. (4), (7), (10) and (13), we can establish the relation between the DC of the refined Bouguer anomaly and the Helmert anomaly as:

$$f_{\mathrm{DC}}(\Delta g_{\mathrm{SRB}}(r,\Omega))=f_{\mathrm{DC}}(\Delta g_{\mathrm{H}}(r,\Omega))+\left.\frac{\partial V_{\mathrm{ct}}(r,\Omega)}{\partial h}\right|_{r=r_{\mathrm{g}}}-\frac{\partial V_{\mathrm{ct}}(r,\Omega)}{\partial h} \tag{14}$$

Note that Vaníček et al. (2004) define another type of gravity anomaly in the so-called "no-topography space." This new type of anomaly is theoretically meaningful, but requires more effort to compute.

3 The degree-banded Stokes integral

In this study, the geoid height N is evaluated in terms of the degree-banded Stokes technique as follows:

$$N(\Omega)=N_{\mathrm{H}}(\Omega)+\delta N_{\mathrm{PITE}}(\Omega)\,, \tag{15}$$

where δN_{PITE}, the primary indirect topographical effect (PITE) on the geoid (Vaníček et al. 1999), is the distance between the geoid and Helmert co-geoid along the normal to the reference ellipsoid. The Helmert co-geoid height N_{H} can be computed by

$$N_{\mathrm{H}}(\Omega)=N^{\mathrm{SG}}_{\mathrm{H},2\sim l}(\Omega)+N^{\mathrm{CG}}_{\mathrm{H},l+1\sim m_{\mathrm{CG}}}(\Omega)+\frac{R}{4\pi\gamma}\int_{\Omega'}S_{\mathrm{DB}}(\psi)\Big[\Delta g^{\mathrm{TG}}_{\mathrm{H}}(\Omega')-\Delta g^{\mathrm{SG}}_{\mathrm{H},2\sim l}(\Omega')-\Delta g^{\mathrm{CG}}_{\mathrm{H},l+1\sim m_{\mathrm{CG}}}(\Omega')\Big]d\Omega'+C_{\mathrm{e}}\,. \tag{16}$$

The subscript H indicates the Helmert field, while the superscripts SG, CG and TG indicate the satellite-only harmonic gravity model, combined harmonic gravity model and terrestrial gravity data, respectively. l represents the selected upper limit for spherical harmonic degree of the satellite-only gravity model. m_{CG} represents the maximum degree of the combined harmonic gravity model, which should preferably be greater than or equal to 200 to properly account for the far-zone contribution of the Stokes integration according to the numerical experiments we have done. Finally, C_{e} represents the residual ellipsoidal correction to the spherical Stokes integration. This correction is omitted in this paper as it accounts for about 2 cm at most in the region of interest (Huang et al. 2003b).

The degree-banded Stokes kernel S_{DB} can be written as:

$$S_{\mathrm{DB}}(\psi) = \sum_{n=l+1}^{m_{\mathrm{TG}}} \frac{2n+1}{n-1} P_n(\cos\psi)\,, \tag{17}$$

where $m_{\mathrm{TG}} = \pi/\Delta$ and Δ corresponds to the sampling interval of the terrestrial gravity data. This modification to Wong and Gore's (1969) kernel truncates the spectral components higher than the data sampling frequency. The truncated kernel eliminates the aliasing errors and can be considered a band-pass weight function to the geoid components. This idea was suggested by Colombo (1977); Novák and Heck (2001) and Kern et al. (2003) applied a similar concept to Poisson's downward continuation and data combination purposes.

A number of modified Stokes kernels (e.g., Meissl 1971; Wenzel 1982; Sjöberg 1984, 1991; Vaníček and Kleusberg 1987; Featherstone et al. 1998; Evans and Featherstone 2000) have been developed with the objective to minimize the far-zone contribution of the Stokes integration and to optimally combine satellite gravity models and terrestrial gravity data. These kernels provide superior alternatives to the degree-banded Stokes kernel (Eq. (17)). However, considering the existence of systematic biases in the Canadian terrestrial gravity anomalies (Véronneau and Huang 2003) and insufficient random error information about them, the degree-banded technique appears to be more practically useful. When the biases and error information become better known, the other kernel modifications cited above may be preferable due to their various theoretical merits.

4 Numerical results in Western Canada

The selected area for numerical investigation is located in Western Canada (latitude 49°N–60°N; longitude 110°W–130°W) and includes the Canadian Rocky Mountains. The topography ranges from sea level to elevations reaching 3,200 m with a mean height of 900 m and a standard deviation of 520 m (see Fig. 1). As stated, Jekeli and Serpas (2003) have already shown that the two approaches produce approximately the same geoid models in areas of plain and hilly topography, but significantly different results in a mountainous area. As such, we shall focus on a mountainous area.

4.1 Gravity data

For the determination of Helmert gravity anomalies on the geoid, we pre-determine an initial gravity grid for both approaches. The initial grid contains refined Bouguer anomalies as defined by Heiskanen and Moritz (1967, Eq. 3–21). The procedure for creating the grid followed four steps:

- evaluate the refined Bouguer anomaly at each terrestrial gravity measurement (land and oceans) using a 1 : 20,000 digital elevation model (DEM) (equivalent to a $1'' \times 1''$ DEM). Terrain corrections were evaluated only within the near-zone with a radius of 50 km using planar formula;
- interpolate the refined Bouguer anomalies into a $40'' \times 40''$ grid by least squares collocation (correlation length: 35 km);
- area-average the refined Bouguer grid onto a $2' \times 2'$ grid; and
- fill the data voids over the oceans by using satellite altimetry-derived gravity data from the NCTU01 model (Hwang et al. 2002).

The far-zone terrain corrections were then added to the refined Bouguer anomalies to produce the spherical refined Bouguer anomalies using the spherical terrain correction formula (Martinec 1998). The Helmert gravity anomalies can be simply summarized from Eqs. (4), (7), (10) and (13) as:

$$\Delta g_{\mathrm{H}}(r_{\mathrm{g}}, \Omega) \doteq \Delta g_{\mathrm{SRB}}(r, \Omega) - \frac{\partial V_{\mathrm{ct}}(r, \Omega)}{\partial h} + f_{\mathrm{DC}}(\Delta g_{\mathrm{H}}(r, \Omega))\,. \tag{18}$$

$$\Delta g_{\mathrm{H}}(r_{\mathrm{g}}, \Omega) \doteq \Delta g_{\mathrm{SRB}}(r, \Omega) + f_{\mathrm{DC}}(\Delta g_{\mathrm{SRB}}(r, \Omega)) - \left.\frac{\partial V_{\mathrm{ct}}(r, \Omega)}{\partial h}\right|_{r=r_{\mathrm{g}}} \tag{19}$$

for approaches A and B, respectively.

4.2 GPS-leveling at benchmarks

The solutions from approaches A and B will be converted to geoid heights (N) and compared with 664 GPS-leveling stations. The GPS-leveling stations are depicted in Fig. 1 as black dots. The geopotential numbers (C) come from a minimum constraint adjustment of the geodetic leveling observations dating after 1981, and three following adjustments by sequentially including leveling observations back to 1971, 1939 and 1904. The rationale behind this strategy is to prevent the older data from distorting the leveling network. The orthometric heights (H) were computed from estimates of real gravity gradients. The national adjustment indicates the observation that the sea level next to Vancouver (Pacific Ocean) is higher than the sea level next to Halifax (Atlantic Ocean) by 80 cm (Véronneau 2002). It is not concluded yet whether the difference represents the sea surface topography, a systematic error over some 6,000 km of leveling lines or a mixture of both. The ellipsoidal heights (h) are obtained from GPS observations between 1986 and 2001 in the ITRF97. The GPS observations also constitute a national adjustment

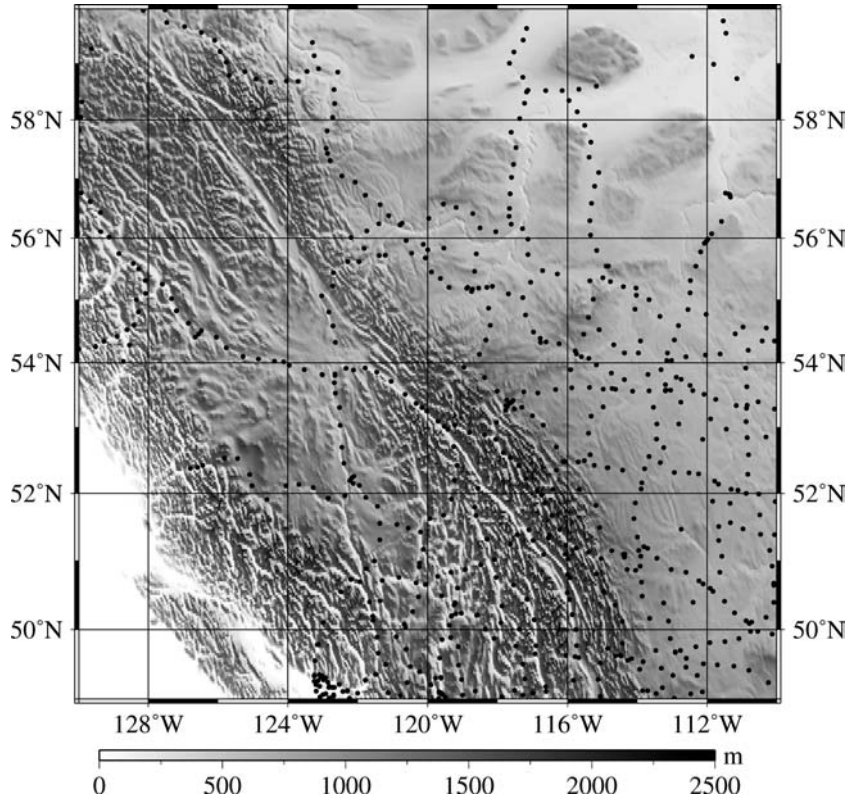

Fig. 1 Topography and the 664 GPS-leveling validation stations in Western Canada

constrained to the active control stations and stations of the Canadian base network (Craymer and Lapelle 2004; pers. comm.).

The relation between the ellipsoidal, geoid and orthometric heights is expressed as:

$$h - H - N \doteq 0\,. \tag{20}$$

The residuals of $h - H - N$ are not expected to be zero because of gross, random and systematic errors in the three height types. The accuracy of geoid heights is usually worse than those of the ellipsoidal and orthometric heights, which are typically precise to between 2 and 5 cm when neglecting possible systematic errors in the leveling network. It should be pointed out that the error might also come from vertical motions (e.g., local subsidence or uplift) at the benchmarks between the leveling and GPS observation epochs.

Geodesists are working towards determining gravimetric geoid heights as accurate as h and H through improved methodologies and data. In most of these developments, GPS-leveling heights ($h - H$) are commonly used to validate the gravimetric geoid heights N and to identify any improvement from methodology and/or data.

4.3 Geoid modeling

As for the terrain correction, the CTE is sensitive to the roughness and resolution of the DEM. The rougher the DEM, the rougher the CTE and, consequently, the Helmert gravity anomalies (see Table 1). However, the determination of the CTE does not require the true DEM because the geoid solution is, in principle, independent of the condensation process, while the terrain correction must be evaluated using a DEM as realistic as possible because the local/regional topography and its composition affect the physical shape of the geoid. The primary role of the mass condensation is to make the PITE small, i.e. to minimize the separation between the geoid and a co-geoid associated with a condensation process. The worst case is the zero-mass condensation that leaves the spherical refined Bouguer anomaly unchanged, and may render the PITE more than 100 m in mountainous regions. The nature of the CTE gives us flexibility to choose a smooth or mean DEM in implementing the Helmert condensation.

The criterion for deciding upon a condensation process is that it yields a smooth gravity anomaly field with a PITE as small as possible on the geoid. From Eq. (18), the CTE is the dominant term in determining the roughness of the Helmert

Table 1 Near-zone contribution (about 110-km radius) of the condensed terrain effect, evaluated at the Earth's surface using the CTED DEM with different resolutions, for the Canadian Rocky Mountains (latitude 49°N–54°N; longitude 114°W–124°W). Unit: mGal

DEM Resolution	Min.	Max.	Mean	Std. Dev.	RMS
$30'' \times 30''$	−163.072	76.129	−2.547	18.885	19.056
$2' \times 2'$	−86.673	50.305	−2.101	12.954	13.123
$5' \times 5'$	−33.407	20.340	−1.176	6.484	6.589

field. For a stable DC, a smooth Helmert field is desired. On the other hand, the PITE tends to increase in magnitude with the condensation of a smoother DEM. A proper choice is that the resolution of the mean DEM, which is used to evaluate the CTE, and that of the gravity data are the same. Therefore, the PITE can be split into two parts. The first part is the primary indirect effect from the DEM for the evaluation of the CTE. The second part takes account of the residual terrain effect that is predictably small. The formulae for the PITE can be found in Appendix B.

Discrete DC of the Helmert gravity anomalies is strongly affected by the CTE. A basic rule is that the DC spatial resolution should be equal to or greater than that of the CTE. Otherwise, the discretization errors become unacceptably large, and may even cause more than 100% of the DC errors (Huang 2002). The discrete DC is also extremely sensitive to the DEM (see Table 2). By increasing the DEM resolution, the DC may even become numerically unstable (Martinec 1996). It turns out that the DC is numerically stable with a mean $2' \times 2'$ DEM in the Canadian Rocky Mountains.

Following approach A, we evaluated geoid heights for Western Canada. It constitutes a region of rough topography and gives among the largest DC effects throughout Canada. The Helmert anomalies were computed by using the near-zone (about 330-km radius) CTE from the mean $2' \times 2'$ CTED DEM and the far-zone CTE from the mean $2^\circ \times 2^\circ$ GTOPO DEM in terms of Eq. (4). The region (latitude 42°N–67°N; longitude 92°W–150°W) is larger than that of the geoid model to reduce the edge effects of the Stokes integration. The DC of the Helmert anomalies was carried out by using Poisson's and Moritz's methods (see Table 3 and Fig. 2).

For Poisson's DC, the integration is carried out over a one-degree cap radius that introduces an accountable truncation error of 1 cm at maximum (Huang 2002). A six-degree cap is used to solve Moritz's DC to order-five so as to meet the convergence of the Moritz DC series. Details of Poisson's and Moritz's methods are not repeated here, since Huang et al. (2003a) review them, among others (e.g. Heiskanen and Moritz 1967; Moritz's 1980; Sideris 1987; Vaníček et al. 1996; Martinec 1996; Jekeli and Serpas 2003).

The regional geoid model was determined via the degree-banded technique described in Sect. 3. The GGMO1C global geopotential model (Tapley et al. 2004) was used to define the long-wavelength part ($l = 30$) of the geoid. The low-degree part of this model (degrees 2 to 90) is determined from the GRACE satellite mission, and the high-degree part (degrees 91 to 200) is determined by combining the GRACE solution with surface gravity data (Ries 2003; personal communication). Our preliminary analysis shows that the GGM01C is significantly better than previous models such as EGM96 within the low-degree band (degrees 2 to 90).

Table 2 Contribution of the downward continuation and the condensed terrain effect within the near-zone (about 110-km radius) using DEMs with different resolutions for the Canadian Rocky Mountains (latitude 49°N–54°N; longitude 114°W–124°W). The CTE is evaluated at the Earth's surface. The band-limited Stokes kernel was used to convert gravity anomalies to geoid heights. Unit: m

Parameter	DEM	Min.	Max.	Mean	SD	RMS
DC	$2' \times 2'$	0.392	1.847	1.240	0.297	1.271
CTE		−1.682	−0.339	−1.120	0.272	1.153
DC + CTE		−0.001	0.233	0.120	0.032	0.124
DC	$5' \times 5'$	0.241	1.024	0.715	0.153	0.731
CTE		0.918	−0.194	−0.612	0.144	0.629
DC + CTE		−0.012	0.213	0.103	0.031	0.108

Table 4 and Fig. 3 show comparisons between the resulting geoid undulations and the GPS-leveling heights at the validation benchmarks. Inclusion of the DC improves the accuracy of the geoid considerably. As shown in Table 3 and Fig. 2, the DC contribution can amount to about 88 mGal in gravity, or 0.5 m in geoid height in the region of study when using the degree-banded Stokes kernel. It is evident that the DC plays a significant role in approach A. The standard deviation of the $h - H - N$ improves from 16.1 to 8.2 cm after adding the Poisson DC to the geoid model. Comparing Figs. 3 b) and c), Poisson's DC gives a greater improvement than Moritz's DC. The result is in agreement with a previous study that suggests an approximation error in Moritz's DC (Huang et al. 2003a).

The DC of the refined Bouguer field is less sensitive to data resolution than the DC of the Helmert gravity field, due to less variability of the Bouguer field. The rows of DC+CTE in Table 2 approximately represent DC of the refined Bouguer field according to Eq. (14). The $5' \times 5'$ DC+CTE differs from the $2' \times 2'$ DC+CTE by only a few centimeters. This suggests that the dominant part of the refined Bouguer DC is characterized by spatial wavelengths longer than $5'$ in this region.

The magnitude of the refined Bouguer DC (about 21 mGal) is significantly smaller than that of the Helmert anomaly DC, as shown in Table 3 and Figs. 2 and 4. However, the DC contribution for approach B is not negligible when the centimeter geoid is sought. Note that the differences between the Poisson and Moritz DC results reach a maximum of about 5 cm in the study region for approach B.

Table 4 shows comparisons between the resulting geoid undulations and the GPS-leveling heights at the validation benchmarks for approach B. The $h - H - N$ results for all three cases of approach B are similar to the one with Poisson's DC for approach A. Improvement in the geoid model is not evident for approach B after the DC is included. The standard deviation of the $h - H - N$ changes from 8.2 to 8.1 cm. It is noticeable that DC does not play an important role in approach B as in approach A. Poisson's DC appears slightly better than Moritz's DC according to results shown in Table 4. The small difference does not tell us if the DC improves the geoid models in approach B because the h and H are typically accurate to about 2–5 cm, and are also affected by vertical motions. For validation purposes, the GPS-leveling data used here are not accurate enough to demonstrate the DC contribution for approach B.

Table 5 shows that the geoid results for the two approaches differ by only a few centimeters, especially when using Poisson's DC. Poisson's DC gives better consistency than Moritz's DC. Figure 5 shows that the small differences are

Table 3 Contribution of the downward continuation effect for the $2' \times 2'$ Helmert and Bouguer gravity fields in Western Canada (latitude 49°N–60°N; longitude 110°W–130°W). The degree-banded Stokes kernel function was used to convert gravity anomalies to geoid heights

Parameter	Approach	DC method	Min.	Max.	Mean	SD	RMS
Gravity	A	Poisson	−49.884	88.091	1.131	8.735	8.808
(mGal)		Moritz	−33.063	61.889	0.960	6.645	6.714
		Poisson - Moritz	−20.864	34.313	0.171	2.496	2.502
	B	Poisson	−20.651	18.346	−0.071	0.973	0.976
		Moritz (g_1 only)	−11.735	12.295	−0.079	0.866	0.869
		Poisson - Moritz	−8.916	6.814	0.007	0.299	0.299
Geoid	A	Poisson	−0.248	0.545	−0.022	0.126	0.128
(m)		Moritz	−0.215	0.462	−0.019	0.107	0.109
		Poisson - Moritz	−0.034	0.098	−0.003	0.019	0.020
	B	Poisson	−0.127	0.052	0.001	0.015	0.015
		Moritz (g_1 only)	−0.166	0.066	0.001	0.023	0.023
		Poisson - Moritz	−0.023	0.054	0.000	0.010	0.010

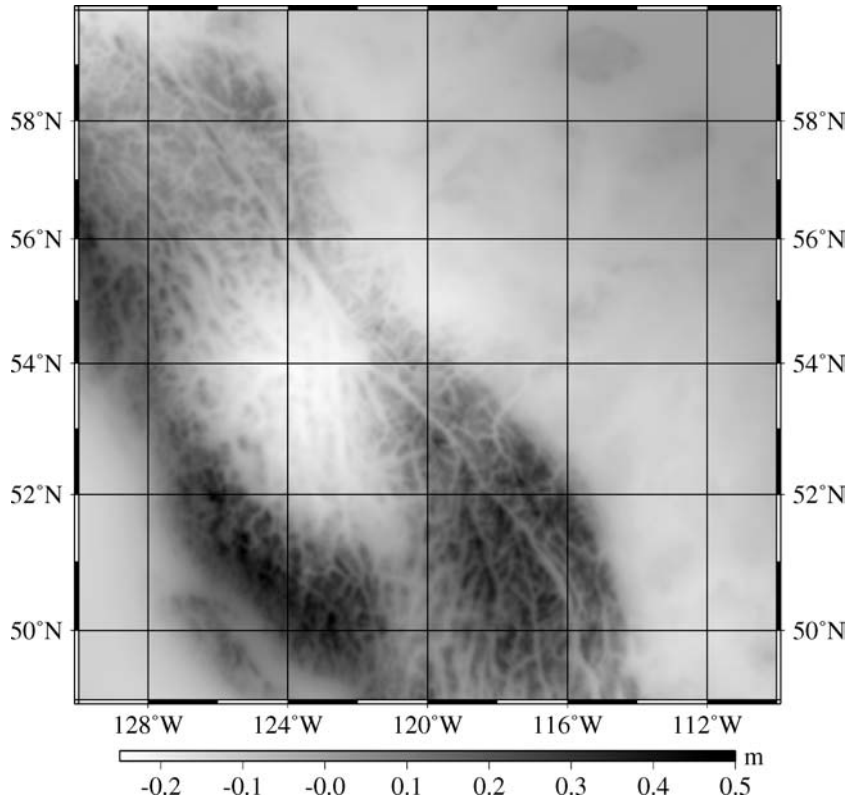

Fig. 2 The downward continuation effect of $2' \times 2'$ Helmert gravity anomalies on the geoid. The degree-banded Stokes kernel function was used to convert gravity anomalies to geoid heights

correlated with the topography shown in Fig. 1, and appear to be attributable to errors in the DC and CTE. Further study is needed to refine the evaluation of the DC and CTE.

5 Summary

Two approaches based on Helmert's second condensation method are applied to determine gravimetric geoid models in Western Canada. Approach A consists of directly continuing the Helmert gravity anomalies downward to the geoid from the Earth's surface, while approach B follows a different procedure in which the refined Bouguer anomalies are continued first, then the Helmert gravity anomalies are formed on the geoid by adding condensation effects. In theory, both approaches are equivalent, but in practice they produce different results due to computational methods and numerical errors.

The DC of the Helmert gravity anomalies is sensitive to the roughness of its field, which is determined principally by the CTE. The roughness of the CTE is directly dependent on the spatial resolution and roughness of the DEM. Fortunately, the geoid model is independent of the condensation process.

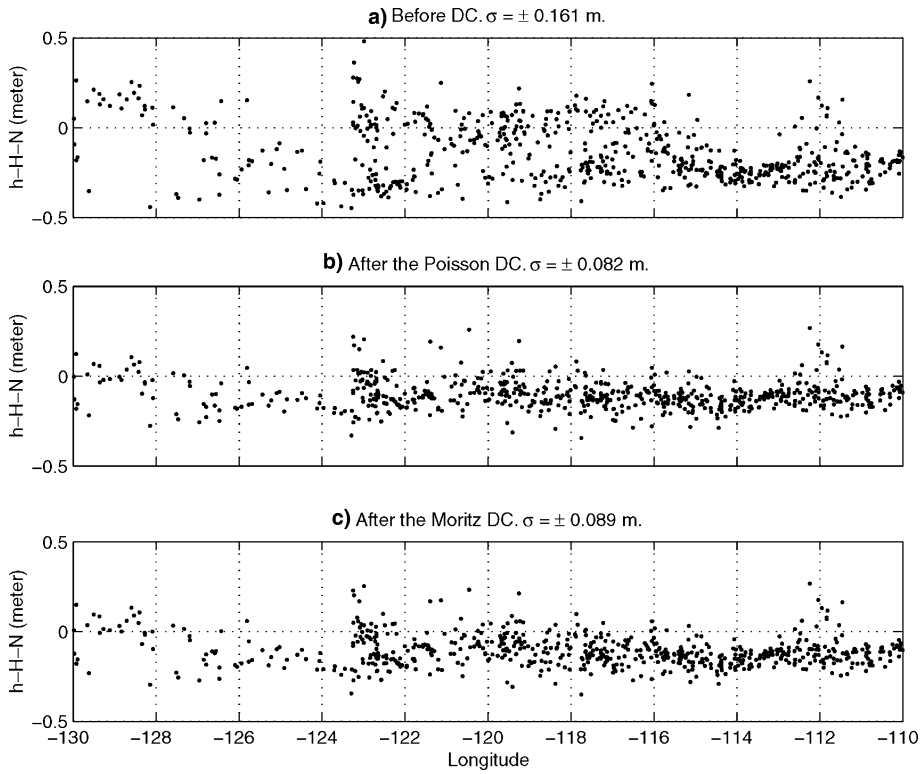

Fig. 3 GPS-leveling versus gravimetric geoid models before and after DC in approach A. h denotes the ellipsoidal height, H denotes the orthometric height, and N denotes the gravimetric geoid height. σ represents standard deviation of the $h - H - N$

This property allows a flexible decision in choosing a smooth or mean DEM for the computation of the CTE. A smooth DEM renders a smooth Helmert gravity field that tends to stablize the DC. However, the smoother the DEM, the larger the PITE. Thus, for DC of the Helmert gravity anomalies, it is important that the mean DEM, used for the determination of the CTE, has the same spatial resolution as the gravity grid. In our case, we use a mean $2' \times 2'$ DEM for the determination of the $2' \times 2'$ Helmert gravity field.

The geoid results from the two approaches were compared to GPS-leveling data in Western Canada. The standard deviations of the $h - H - N$ for both approaches are about 8 cm at 664 GPS-leveling validation stations in Western Canada. Approach A is more sensitive to DC because of the roughness of the Helmert gravity field. The DC effects of the Helmert gravity anomalies on the geoid reach up to about 0.5 m in Western Canada when the degree-banded Stokes kernel is used. Poisson's DC provides better numerical results than Moritz's DC for approach A in terms of validation against the GPS-leveling. Approach B is less sensitive to DC because of the smoothness of the refined Bouguer gravity field. The DC of the refined Bouguer anomalies contributes to the geoid at the decimeter level in Western Canada, but the accuracy of h and H imposes limitations on validating this contribution. Both Poisson's and Moritz's DC give similar geoid results when validated against the GPS-leveling for approach B. The numerical differences between approaches A and B account for a few centimeters. They are mainly attributed to the numerical accuracy of the DC and CTE. Note that Jekeli and Serpas (2003) showed significant differences of the geoid heights between the two approaches in their mountainous region. The differences may be caused by the insufficient resolution of the DC in contrast to that of the CTE in their computations.

Table 4 Statistics of the $h - H - N$ with and without the DC for approaches A and B at the 664 GPS-leveling stations in Western Canada. Unit: m

Approach	DC method	Min.	Max.	Mean	SD
A	Not Applied	−0.447	0.482	−0.142	0.161
	Poisson	−0.343	0.267	−0.103	0.082
	Moritz	−0.350	0.266	−0.107	0.089
B	Not Applied	−0.362	0.276	−0.099	0.082
	Poisson	−0.358	0.267	−0.103	0.081
	Moritz	−0.345	0.268	−0.105	0.083

Table 5 Gravity and geoid differences between approaches A and B for the same DC method in Western Canada (latitude 49°N–60°N; longitude 110°W–130°W). 198,000 points

Parameter	DC methods	Min.	Max.	Mean	SD	RMS
Gravity	Poisson	−4.128	5.871	−0.051	0.310	0.314
(mGal)	Moritz	−39.196	20.220	−0.215	2.442	2.442
Geoid	Poisson	−0.050	0.033	0.000	0.009	0.009
(m)	Moritz	−0.088	0.029	0.003	0.019	0.019

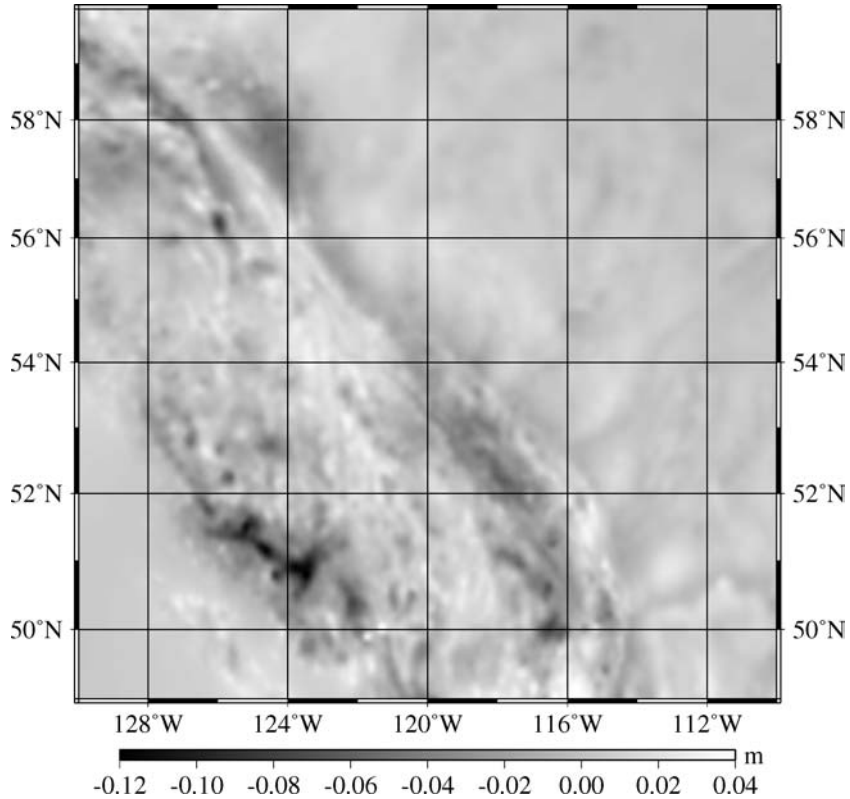

Fig. 4 The downward continuation effect of the $2' \times 2'$ refined Bouguer gravity anomalies on the geoid using Poisson's equation. The degree-banded Stokes kernel function was used to convert gravity anomalies to geoid heights. Note the grayscale for this figure is different to that of Fig. 2 to show the features

Acknowledgements We want to express our appreciation to Prof. Will Featherstone, Prof. Chris Jekeli and two anonymous reviewers for their critical remarks. We gratefully thank Dr. Nico Sneeuw of the University of Calgary, Drs. Calvin Klatt and André Mainville at Geodetic Survey Division, Canada Center for Remote Sensing, Natural Resources Canada, and Dr. Artu Ellmann at the University of New Brunswick for their comments. GMT was used to produce the figures (Wessel and Smith 1998).

Appendix

A Condensed topographical effect (CTE)

$$\begin{aligned}\mathrm{CTE} &= -\frac{\partial V_{\mathrm{ct}}(r,\Omega)}{\partial h} \\ &\doteq 4\pi G\sigma(\Omega))\frac{R^2}{r^2} - GR^2 \\ &\quad \times \int_{\Omega'} [\sigma(\Omega') - \sigma(\Omega)]\frac{\partial L^{-1}(r,\psi,r')}{\partial r} d\Omega' \end{aligned} \tag{21}$$

where

$$L(r,\psi,r') = (r^2 - 2rr'\cos\psi + r'^2)^{\frac{1}{2}} \tag{22}$$

$$\sigma(\Omega) \doteq \overline{\rho}(\Omega)H(\Omega) \tag{23}$$

B Primary indirect topographical effect (PITE)

$$\delta N_{\mathrm{PITE}}(\Omega) = \frac{\delta V_1(\Omega)}{\gamma} + \frac{\delta V_2(\Omega)}{\gamma} \tag{24}$$

where

$$\begin{aligned}\delta V_1(\Omega) &= V_{\mathrm{cap}}(\Omega) - V_{\mathrm{ccap}}(\Omega) \\ &\quad + G\int_{\Omega'_0}\Big[\overline{\rho}(\Omega')\tilde{K}\left(R,\psi,r'\right)\Big|_{r'=R}^{R+H(\Omega')} \\ &\quad - \overline{\rho}(\Omega)\tilde{K}\left(R,\psi,r'\right)\Big|_{r'=R}^{R+H(\Omega)}\Big] d\Omega' \\ &\quad - G\int_{\Omega'_0} R^2[\overline{\rho}(\Omega')\tau(H(\Omega')) \\ &\quad - \overline{\rho}(\Omega)\tau(H(\Omega))]L^{-1}(R,\psi,R)d\Omega' \\ &\quad + G\int_{\Omega'-\Omega'_0}\overline{\rho}(\Omega')\Big[\tilde{K}\left(R,\psi,r'\right)\Big|_{r'=R}^{R+H(\Omega')} \\ &\quad - R^2\tau(H(\Omega'))L^{-1}(R,\psi,R)\Big] d\Omega' \end{aligned} \tag{25}$$

$$\begin{aligned}\tilde{K}(r,\psi,r') &= \frac{1}{2}(r' + 3r\cos\psi)L(r,\psi,r') \\ &\quad + \frac{r^2}{2}(3\cos^2\psi - 1)\ln|r' - r\cos\psi \\ &\quad + L(r,\psi,r')| + C \end{aligned} \tag{26}$$

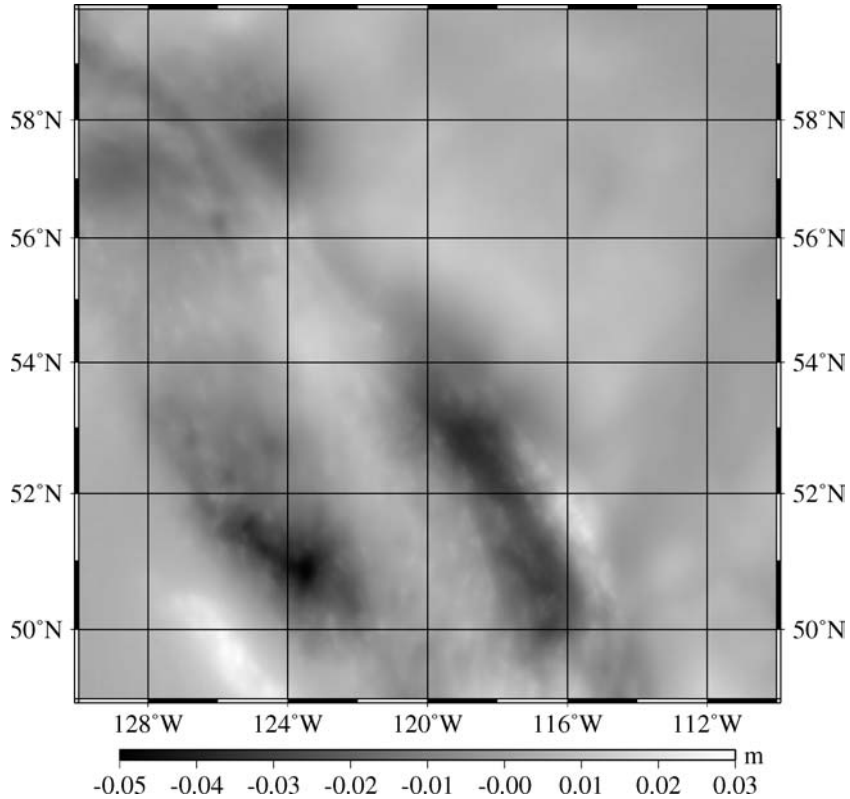

Fig. 5 Geoid height differences between approaches A and B with the Poisson DC. Note the grayscale for this figure is different to that of Figs. 2 and 4 to show the features

$$\tau(H) = H\left(1 + \frac{H}{R} + \frac{H^2}{3R^2}\right) \tag{27}$$

$$\begin{aligned} V_{\text{cap}}(\Omega) = {} & 2\pi G\overline{\rho}(\Omega) \\ & \times \left[\left(-\frac{(3\cos^2\psi - 2)R}{6} - \frac{r'\cos\psi}{6} + \frac{r'^2}{3R}\right)\right. \\ & \times L(R,\psi,r') \\ & -\frac{1}{2}R^2(\cos^3\psi - \cos\psi) \\ & \left.\times \ \ln\left(-R\cos\psi + r' + L(R,\psi,r')\right)\right]\Bigg|_{\psi=0}^{\psi=\psi_0}\Bigg|_{r'=R}^{R+H(\Omega)} \end{aligned} \tag{28}$$

$$V_{\text{ccap}}(\Omega) = 4\pi G R\overline{\rho}(\Omega)\tau(H(\Omega))\sin\frac{\psi_0}{2} \tag{29}$$

$$\delta V_2(\Omega) = G\int_{\Omega'}\overline{\rho}(\Omega')\tilde{K}(R,\psi,r')\Big|_{r'=R+H(\Omega')}^{R+H(\Omega')+\delta H(\Omega')} d\Omega' \tag{30}$$

References

Bjerhammar A (1987) Discrete physical geodesy. Report no. 380, Department of Geodetic Science and Surveying, Ohio State University, Columbus

Colombo OL (1977) Optimal kernels for band-limited data. Unisurv G27, University of New South Wales, Sydney

Engels J, Grafarend E, Keller W, Martinec Z, Sansò R, Vaníček P (1993) The geoid as an inverse problem to be regularized. In: Anger G, Gorenflo R, Jochmann H, Moritz H, Webers W (eds) Inverse problems: Principles and applications in geophysics, technology and medicine, Akademie Verlag, Berlin, pp. 122–167

Evans JD, Featherstone WE (2000) Improved convergence rates for the truncation error in geoid determination. J Geod 74:239–248

Featherstone WE, Evans JD, Olliver JG (1998) A Meissl-modified Vaníček and Kleusberg kernel to reduce the truncation error in gravimetric geoid computations. J Geod 72:154–160

Featherstone WE, Kirby JF, Kearsley AHW, Gilliland JR, Johnston GM, Steed J, Forsberg R, Sideris MG (2001) The AusGeoid98 geoid model of Australia: data treatment, computations and comparisons with GPS-leveling data. J Geod 75:313–330

Heck B (2003) On Helmert's methods of condensation. J Geod 77:155–170

Heiskanen WA, Moritz H (1967) Physical geodesy. W.H. Freeman, San Francisco

Huang J (2002) Computational methods for the discrete downward continuation of the Earth gravity and effects of lateral topographical mass density variation of gravity and geoid. GGE Technical report 216, Deptartment of Geodesy and Geomatics Engineering, University of New Brunswick, Fredericton

Huang J, Sideris MG, Vaníček P, Tziavos IN (2003a) Numerical investigation of downward continuation for gravity anomalies. Bolletino Di Geodesia E Scienze Affini LXII(1):33–48
Huang J, Véronneau M, Pagiatakis SD (2003b) On the ellipsoidal correction to the spherical Stokes solution of the gravimetric geoid. J Geod 77:171–181
Hwang C, Hsu HY, Jiang RJ (2002) Global mean sea surface and marine gravity anomaly from multi-satellite altimetry: applications of deflection-geoid and inverse Vening Meinesz formulae. J Geod 76:407–418
Ilk KH, Kusche J, Rudolph S (2002) A contribution to data combination in ill-posed downward continuation problems. J Geod 33:75–99
Jekeli C (1981) The downward continuation to the Earth's surface of truncated spherical and ellipsoidal harmonic series of the gravity and height anomalies. Report no. 323, Deptartment of Geodetic Science and Surveying, Ohio State University, Columbus
Jekeli C, Serpas JG (2003) Review and numerical assessment of the direct topographical reduction in geoid determination. J Geod 77:226–239
Kern M, Schwarz KP, Sneeuw N (2003) A study on the combination of satellite, airborne, and terrestrial gravity data. J Geod 77:217–225
Martinec Z, Matyska C, Grafarend EW, Vaníček P (1993) On Helmert's second condensation technique. Manuscr Geod 19:213–219
Martinec Z (1996) Stability investigations of a discrete downward continuation problem for geoid determination in the Canadian Rocky Mountains. J Geod 70:805–828
Martinec Z (1998) Boundary-value problems for gravimetric determination of a precise geoid. Lecture notes in Earth sciences 73, Springer, Berlin Heidelberg New York
Meissl P (1971) Preparations for the numerical evaluation of second-order Molodensky-type formulas. Report no. 163, Department of Geodetic Science, Ohio State University, Columbus
Milbert D (1999) The dilemma of downward continuation. AGU 1999 spring meeting, 1–4 June, 1999, Boston
Moritz H (1968) On the use of the terrain correction in solving Molodensky's problem. Report 106, Department of Geodesy Science Ohio State University, Columbus
Moritz H (1980) Advanced Physical Geodesy. Herbert Wichmann Verlag, Karlsruhe
Nahavandchi H (2000) The direct topographical correction in gravimetric geoid determination by the Stokes-Helmert method. J Geod 74:488–496
Novák P, Heck B (2001) Downward continuation and geoid determination based on band-limited airborne gravity data. J Geod 76:269–278
Omang OCD, Forsberg R (2000) How to handle topography in practical geoid determination: three examples. J Geod 74:458–466
Rummel R, Schwarz KP, Gerstl M (1979) Least squares collocation and regularization. Bull Géod 53:343–361
Schwarz KP (1978) Geodetic improperly posed problems and their regularization. Lecture notes of the 2nd International school of advanced geodesy, Erice
Sideris MG (1987) Spectral methods for the numerical solution of Molodensky's problem. UCSE Report 20024. Department of Surveying Engineering University of Calgary, Calgary
Sideris MG (1994) Geoid determination by FFT techniques. Lecture notes for international school for the determination and use of the Geoid, Milan, 10–15 October, 1994
Sjöberg LE (1984) Least-squares modification of Stokes's and Vening Meinesz's formula by accounting for truncation and potential coefficient errors. Manuscr Geod 9:229–248
Sjöberg LE (1991) Refined least squares modification of Stokes's formula. Manuscr Geod 12:86–98
Sjöberg LE (1996) On the error of analytical continuation in physical geodesy. J Geod 70:724–730
Sjöberg LE (1998) The exterior Airy/Heiskanen topographic-isostatic gravity potential anomaly and the effect of analytical continuation in Stokes's formula. J Geod 72:654–662
Sjöberg LE (2003) A solution to the downward continuation effect on the geoid determined by Stokes's formula. J Geod 77:94–100
Smith DA, Milbert D (1999) The GEOID96 high resolution geoid height model for the United States. J Geod 73:219–236
Sun W, Vaníček P (1998) On some problems of the downward continuation of the $5' \times 5'$ mean Helmert gravity disturbance. J Geod 72:411–420
Tapley BD, Bettadpur S, Watkins M, Reigber Ch (2004) The gravity recovery and climate experiment: mission overview and early results. Geophys Res Lett 31, L09607: DOI 10.1029/2004GL019920
Vaníček P, Kleusberg A (1987) The Canadian geoid—Stokesian approach. Manuscr Geod 12:86–98
Vaníček P, Martinec Z (1994) The Stokes-Helmert scheme for the evaluation of a precise geoid. Manuscr Geod 19:119–128
Vaníček P, Sun W, Ong P, Martinec Z, Najafi M, Vajda P, Ter Horst B (1996) Downward continuation of Helmert's gravity anomaly. J Geod 71:21–34
Vaníček P, Huang J, Novák P, Pagiatakis SD, Véronneau M, Martinec Z, Featherstone WE (1999) Determination of the boundary values for the Stokes-Helmert problem. J Geod 73:180–192
Vaníček P, Tenzer R, Sjöberg LE, Martinec Z, Featherstone WE (2004) New views of the spherical Bouguer gravity anomaly. Geophys J Int 159:460–472
Véronneau M (1997) The GSD95 geoid model of Canada. In: Segawa J, Fujimoto H, Okubo S (eds) Gravity, Geoid and Marine Geodesy, Springer, Berlin Heidelberg New York, pp 573–580
Véronneau M (2002) Canadian gravimetric geoid model of 2000 (CGG2000). Report, Geodetic Survey Division, Natural Resources Canada, Ottawa, Ontario
Véronneau M, Huang J (2003) Correction of systematic errors in surface gravity anomalies using satellite gravity solutions. In: Tziavos IN (ed) Gravity and Geoid, ZITI publications, Thessaloniki, pp 217–222
Wang YM (1988) Downward continuation of the free-air gravity anomalies to the ellipsoid using the gradient solution, Poisson's integral and terrain correction - numerical comparison of computations. Report no. 393, Department of Geodetic Science and Surveying, Ohio State University, Columbus
Wenzel HG (1982) Geoid computation by least-squares spectral combination using integration kernels. In: Nakagawa I, Kasahara K, Tanaka T (eds) Proceedings of the IAG general meeting, Tokyo, The Geodetic Society of Japan, pp 438–453
Wessel P, Smith WHF (1998) New, improved version of generic mapping tools released, EOS Trans Amer Geophys Union 79(47):579
Wong L, Gore R (1969) Accuracy of geoid heights from modified Stokes kernel. Geophys J R Astron Soc 18:81–91
Wong JCF (2001) On Picard criterion and the well-posed nature of harmonic downward continuation. GGE technical report 213, Department of Geodesy and Geomatics Engineering, University of New Brunswick, Fredericton